

# Catalysis Science & Technology

Accepted Manuscript



This article can be cited before page numbers have been issued, to do this please use: Y. Chai, J. Lu, L. Li, D. Li, M. Li and J. Liang, *Catal. Sci. Technol.*, 2018, DOI: 10.1039/C8CY00274F.



This is an Accepted Manuscript, which has been through the Royal Society of Chemistry peer review process and has been accepted for publication.

Accepted Manuscripts are published online shortly after acceptance, before technical editing, formatting and proof reading. Using this free service, authors can make their results available to the community, in citable form, before we publish the edited article. We will replace this Accepted Manuscript with the edited and formatted Advance Article as soon as it is available.

You can find more information about Accepted Manuscripts in the [author guidelines](#).

Please note that technical editing may introduce minor changes to the text and/or graphics, which may alter content. The journal's standard [Terms & Conditions](#) and the ethical guidelines, outlined in our [author and reviewer resource centre](#), still apply. In no event shall the Royal Society of Chemistry be held responsible for any errors or omissions in this Accepted Manuscript or any consequences arising from the use of any information it contains.



Journal Name

ARTICLE

## TEOA-induced in situ formation of wurtzite and zinc-blende CdS heterostructures as a high-active and long-lasting photocatalyst for converting CO<sub>2</sub> into solar fuel

Yao Chai, Jiaxue Lu, Li Li,\* Deli Li, Meng Li and Jun Liang\*

Received 00th January 20xx,  
Accepted 00th January 20xx

DOI: 10.1039/x0xx00000x

www.rsc.org/

The wurtzite and zinc-blende CdS heterostructures are designed and *in situ* synthesized by tuning triethanolamine (TEOA) usage in a mild hydrothermal condition. The as-prepared samples were systematically characterized by XRD, SEM, TEM, UV-vis DRS, XPS, PL, and Mott-Schottky. It is realized that a further increase in used amount of TEOA promote the CdS phase transformation from hexagonal wurtzite to cubic zinc-blende during hydrothermal process, and detailed investigations indicate that the heteronanoparticles possess explicit heterointerfaces and strong light absorption as well as tunable band gaps. Especially when used as photocatalyst toward reduction of CO<sub>2</sub> to CO and CH<sub>4</sub> in the presence of H<sub>2</sub>O, the heterostructured CdS hybrids display not only better photocatalytic CH<sub>4</sub>-/CO-producing activity under visible-light irradiation than that of isolated CdS phase, but also unprecedented cycling stability, without hardly deactivation over 100 h. The remarkable improvement of photoactivity and stability over CdS-based hybrid can be attributed to better electron-hole pair separation and migration owing to junctions formed by coexistence of wurtzite and zinc-blende in the CdS nanostructures, according to the physicochemical characterization. Additionally, the role of the junctions endowed by wurtzite/zinc-blende CdS in the process of the CO<sub>2</sub> photoreduction is evaluated by using transient photocurrents and electrochemical impedance spectra (EIS) analysis, illustrating its fast-interfacial charge transfer. This work would provide a significant avenue to effectively photocatalytic conversion CO<sub>2</sub> using rationally designed CdS-based surface phase junctions engineering at nanoscale..

### 1. Introduction

Semiconductor-based heterogeneous photocatalysis was seen as a potential solution for CO<sub>2</sub> conversion to produce solar fuels (e.g., CO, CH<sub>4</sub>, HCOOH, CH<sub>3</sub>OH, C<sub>2</sub>H<sub>5</sub>OH) through the reaction of CO<sub>2</sub> reduction with H<sub>2</sub>O.<sup>1</sup> To achieve this, numerous studies have been made to improve the CO<sub>2</sub> conversion efficiency through developing highly active photocatalysts. However, a troublesome issue for these photocatalytic materials is their limited charge separation efficiency, low sunlight harvesting, and poor photostability, which has largely hindered their practical applications in this field.<sup>2</sup> CdS, a narrow bandgap (E<sub>g</sub> = 2.4 eV) semiconductor, has a valence band edge, which is positioned more positive (vs. NHE) than the H<sub>2</sub>O/O<sub>2</sub> oxidation potential, and a conduction band edge is more negative than the reduction potential for CO/CO<sub>2</sub>,<sup>3-6</sup> which make it an ideal candidate as visible-light-driven photocatalyst for efficiently converting CO<sub>2</sub> into

renewable solar fuels in the presence of H<sub>2</sub>O. Unfortunately, a major problem on CdS is high-rate recombination of charge carriers and low photostability.<sup>7,8</sup>

To overcome the obstacle of low charge separation efficiency and stability of CdS during CO<sub>2</sub> photoreduction process, many strategies have been proposed including loading cocatalysts,<sup>9-12</sup> integration with carbon-based materials,<sup>13-16</sup> and semiconductor coupling,<sup>17-20</sup> etc. However, these methods for improved photocatalytic reduction of CO<sub>2</sub> are not yet satisfactory.

Recently, surface-phase junctions deduced by the same semiconductor (e.g.,  $\alpha$ -/ $\beta$ -Ga<sub>2</sub>O<sub>3</sub>, *h*-/*m*-BiVO<sub>4</sub>, or  $\alpha$ -/ $\beta$ -Bi<sub>2</sub>O<sub>3</sub> junctions)<sup>21-24</sup> has been proven to be useful for enhancing photocatalytic performance, which is clearly revealing to be a very effective approach for retarding electron-hole pair recombination. As a competitive semiconductor, CdS generally exists in two different crystalline phases including the wurtzite and zinc-blende. As compared to zinc-blende CdS, the wurtzite CdS has been concerned more intensively because it owns relatively good photoability and can be achieved readily by different synthetic methods.<sup>25</sup> Therefore, the wurtzite CdS coupled with other semiconductors have been studied largely.<sup>26-29</sup>

But so far, only a few procedures were contributed to prepare CdS heterostructure-based phase junction and its limited application in photocatalysis is also merely based on

State Key Laboratory of High-efficiency Utilization of Coal and Green Chemical Engineering, College of Chemistry and Chemical Engineering, Ningxia University, Yinchuan 750021, China.

E-mail: Junliang@nxu.edu.cn; li\_l@nxu.edu.cn.

Footnotes relating to the title and/or authors should appear here.

Electronic Supplementary Information (ESI) available: [Figures of XRD patterns, TEM images, photocatalytic activities]. See DOI:10.1039/x0xx00000x

water splitting to produce hydrogen.<sup>8, 30-32</sup> Moreover, according to these studies, the discrepancy in photocatalytic activities<sup>5, 30-32</sup> also indicated that fabrication of noble metal-free CdS-based high-quality phase junction with intimate heterointerfaces is lacking and its precise synthesis is still a big challenge. Additionally, no reports on CdS-based heterostructures are available on converting CO<sub>2</sub> into solar fuel by photocatalytic technology.

Herein, we developed a highly facile hydrothermal approach to construct wurtzite/zinc-blende CdS heterostructures with tunable heterointerfaces by a general TEOA-mediated one-step hydrothermal method, and the CdS surface-phase junction is first applied in visible-light-driven photocatalytic CO<sub>2</sub> reduction conjugated with H<sub>2</sub>O oxidation. Meanwhile, excellent CH<sub>4</sub>- and CO-producing rate (0.31 and 1.61 μmol h<sup>-1</sup> g<sup>-1</sup>) and outstanding photostability (the stability test over 100 h) were also achieved. It was found that the surface-phase junction between wurtzite and zinc-blende CdS is responsible for the enhanced photocatalytic activity and excellent cycling stability, which promotes the charge transfer in the reaction process and makes the photo-generated electrons important role in the photoreduction process.

## 2. Experimental

### 2.1 Materials and preparation

All the chemicals used in the experiment were of analytical grade and used without further purification. A series of photocatalysts was prepared by a simple hydrothermal method. First, different amount of triethanolamine (TEOA) and 1 mmol of CdCl<sub>2</sub>·2.5H<sub>2</sub>O were added in turn into 18 ml of deionized water to form solution with vigorous stirring. Then, 4 mmol of thioacetamide was dissolved into the above mixture solution. The yellow slurry was further stirred for 30 min under ambient temperature. The resulting mixture is finally transferred to a 30-mL Teflon-lined stainless-steel autoclave, sealed and kept at 180 °C for 3 h. After the reaction completed, the yellow solid precipitate was separated by centrifugation and washed many times with distilled water and anhydrous ethanol. The product was dried under vacuum at 60 °C for 12 h. Additionally, appropriate amount of other inorganic base or organic base (e.g. ammonia (NH<sub>3</sub>·H<sub>2</sub>O), ethylene diamine (EDA), NaOH) instead of TEOA were introduced to the hydrothermal system, and the as-obtained CdS samples are also characterized and tested.

### 2.2 Characterization

The crystal structure of the sample was characterized by X-ray powder diffraction (XRD) in a Bruker D8 Advance X-ray diffractometer with Cu Kα radiation (λ=0.15406 nm) operating at 40 kV and 40 mA with a scanning rate of 0.02° per second from 5° to 80°. The morphologies and sizes of the samples were examined by field-emission scanning electron microscopy (FE-SEM, JEOL JSM - 6701F). The chemical structure, morphology, and energy-dispersive spectroscopy (EDS) of the sample were characterized using a JEOL model JEM 2010 EX

microscope at an accelerating voltage of 200 kV. The surface chemical compositions of samples were analysed by X-ray photoelectron spectroscopy with an ESCALAB 250 XPS electron spectrometer with a mono-achromatized Al Kα X-ray source. The binding energy was referenced to the C 1s peak at 284.8 eV. The optical absorption property of sample was recorded by ultraviolet-visible diffuse reflectance spectra (UV-Vis DRS) on a Varian Cary 500 Scan UV/Vis system, in which BaSO<sub>4</sub> was used as the background. The photoluminescence (PL) spectra were analyzed using an FL 920 spectrometer (Edinburgh Instrument).

### 2.3 Photocatalytic testing

The photocatalytic activities of the as-obtained CdS samples were evaluated for the photocatalytic reduction of CO<sub>2</sub> under visible-light irradiation. In a typical experiment, 20 mg of the as-prepared photocatalyst was firstly loaded into a 25 mL pyrex glass reactor. Subsequently, the whole system was subjected to vacuum degassing and then backfilling with pure CO<sub>2</sub> gas. This process was repeated several times, and after the last cycle the reactor was backfilled with CO<sub>2</sub> (1 bar). Finally, 10 μL of deionized water was introduced into the reactor with a syringe, and deionized water was gasified by heating. A 300 W Xe lamp was used with cut-off filter to provide visible light (≥420 nm). Prior to irradiation, stirring in dark for 1 h was allowed for establishment of adsorption/desorption equilibrium. The photocatalytic reaction was carried out for 5 h under visible light irradiation (λ≥420 nm). Finally, 0.5 mL of gas was taken from the glass reactor for subsequent gas concentration analysis using a gas chromatography (GC-7890A, Shimadzu) equipped with a flame ionized detector (FID). Product gases were calibrated with a standard gas mixture and their identity determined using the retention time.

### 2.4 Photoelectrochemical measurements

Photoelectrochemical measurements were carried out with a BAS Epsilon workstation using a standard three-electrode electrochemical cell with a working electrode, a platinum foil as the counter electrode, and a saturated Ag/AgCl electrode as the reference. A sodium sulfate solution (0.2 M) was used as the electrolyte, and a 300 W xenon lamp was introduced as the light source. The working electrode was prepared by FTO glass pieces, which was cleaned by sonication in cleanout fluid, acetone and ethanol in sequence. The photocatalyst was dispersed in ethanol under sonication to form a suspension. A photocatalyst film was fabricated by spreading the suspension onto the conductive surface of the FTO glass.

## 3. Results and discussion

The mixed-phase CdS surface-phase junction was obtained by treating CdCl<sub>2</sub>·2.5H<sub>2</sub>O and thioacetamide solution at 180°C with controlled TEOA dosages and reaction times, and the effects of the TEOA dosages and the hydrothermal reaction time on crystallization process were examined by XRD. Fig. 1a shows the XRD patterns of the products prepared at different amounts of TEOA. It can be observed that diffraction peaks of

sample prepared in the absence of TEOA are well-indexed to the pure hexagonal wurtzite CdS (JCPDS card No. 41-1049) (indicated as HS-0). However, of all the samples synthesized under different amount of TEOA, diffraction peaks at  $26.5^\circ$  and  $30.6^\circ$  corresponding to the cubic zinc-blende CdS (JCPDS card No. 10-0454) in comparison to the HS-0 are detected, suggesting that introduction of TEOA is favourable for CdS in situ phase transformation from hexagonal wurtzite to cubic zinc-blende. As to be observed later, increasing the used amount of the TEOA from 0.1 g to 2.0 g, the intensities of the diffraction peaks for hexagonal wurtzite located at  $28.2^\circ$ ,  $36.6^\circ$  and  $47.8^\circ$  decrease gradually, whereas the diffraction peaks for cubic zinc-blende centered at  $26.5^\circ$  and  $30.6^\circ$  increases continually (shown with arrow in Fig. 1a). The results indicate that the phase transformation has been undergoing from wurtzite to zinc-blende by ranging the TEOA dosage (denoted as HCS-n,  $n_{\text{TEOA dosage}} = 0.3, 1.0, 2.0$  g). Furthermore, with the further increase of the TEOA amount up to 5.0 g, this concludes the high-percentage of the zinc-blende CdS in the overall crystals, while very small amount of second phase can be assigned to hexagonal phase of wurtzite CdS (denoted as

CS-5). According to these XRD results, indicating that the nanoheterostructured wurtzite/zinc-blende CdS hybrids could be easily tuned under present hydrothermal conditions, while TEOA is essential for formation and transformation of junctions between wurtzite and zinc-blende CdS. This might be because weak basic system endowed by TEOA adjusts the dissociation rate of thioacetamide, that is to say, dissociation and diffusion rates based on the competitively reaction kinetics of between metal cations and sulphide anions assisted by  $\text{OH}^-$  could boost the phase transformation from wurtzite to zinc-blende during the sulfidation process. To further identify the role of TEOA, appropriate amount of other inorganic base or organic base (e.g. ammonia, ethylene diamine, NaOH) instead of TEOA were used, and the mixed-phase CdS samples were also obtained (Fig. 2). These results clearly suggested that the formation of the mixed-phase CdS surface-phase junctions mainly depends on the present weak basic hydrothermal system, that is, the general control can be achieved by adding alkali liquors such as TEOA, En, etc to prepare heterostructured CdS hybrids.

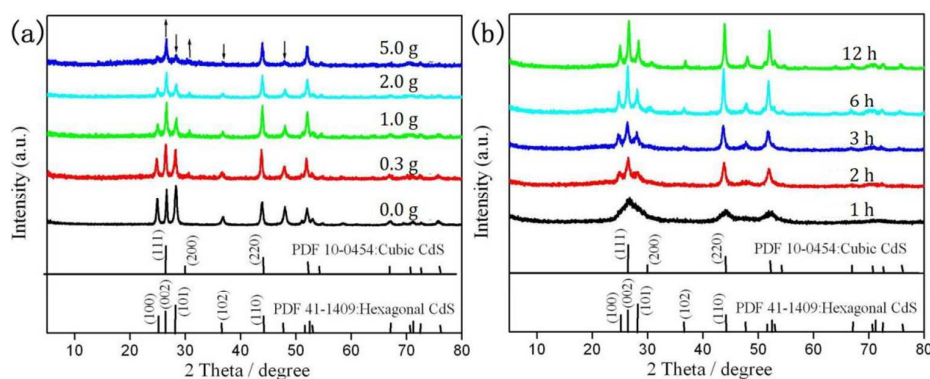


**Fig. 1** The XRD patterns of the samples prepared at  $180^\circ\text{C}$  under different (a) TEOA amount and (b) hydrothermal treatment time, respectively.

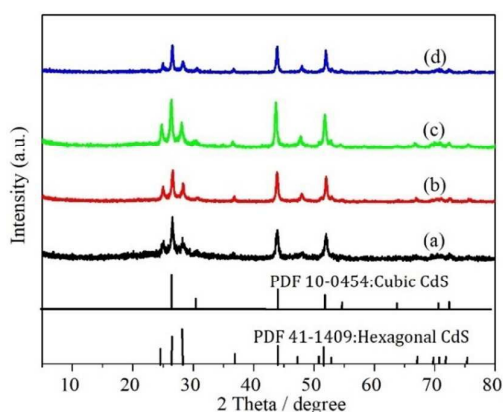


**Fig. 2** The XRD patterns of the samples prepared in the presence of (a) TEOA, (b) EDA, (c)  $\text{NH}_3\text{H}_2\text{O}$ , and (d) NaOH.

Additionally, hydrothermal treatment time is also a very influential factor in formation of CdS surface-phase junction.

As to be shown in Fig. 1b and Fig. S1, cubic zinc-blende CdS obtained in less than an hour displays characteristic X-ray diffraction peaks that are representative of semi-amorphous semiconductor materials. Afterward, increasing the reaction time from 1 h to 12 h, we observe that the diffraction peaks of zinc-blende CdS on intensity decrease gradually, whereas the intensity of diffraction peaks for wurtzite CdS increases slowly. This result shows that wurtzite CdS can be in situ transformed from zinc-blende CdS with the increase of the hydrothermal treatment time. On the basis of above analysis (Fig. 1 and Fig. 2), demonstrating that the weak alkaline surroundings induced by TEOA or other alkali liquors easily leads to formation of mixed-phase CdS heterojunctions in the current hydrothermal system, and the hydrothermal treatment time can be effectively applied to control the phase transformation process from zinc-blende to wurtzite in the hydrothermal condition of  $180^\circ\text{C}$ .

The crystalline microstructure of heterostructured CdS based sample (HCS-1) was provided by TEM and SEM. From

Fig. 3a and 3b, the low magnification TEM and SEM images reveal that HCS-1 is composed of a large number of uniform nanoparticles, with sizes ranging from 20 to 40 nm. To verify the heterostructure proposed by XRD results, high resolution transmission electron microscopy (HRTEM) characterization was performed. As presented in Fig. 3c, it can be clearly seen that the highly crystalline heterointerface between wurtzite and zinc-blende crystalline phase can be readily obtained. Meanwhile, the interplanar *d* spacing of 0.316 nm is in good agreement with that of the (101) plane of hexagonal wurtzite CdS, and the *d* spacing of 0.336 nm is also assigned to that of the cubic zinc-blende CdS (111) planes in the mixed-phase CdS hybrid, indicating the formation of CdS-based surface-phase

junctions in the nano hybrids. In addition, the chemical composition of the sample was characterized by energy-dispersive X-ray spectroscopy (EDX). As shown insert in the Fig. 3d, the sample is composed of Cd and S and the atomic ratio of Cd to S is ca. 1.01, which is consistent with the stoichiometric value for CdS. The selected area electron diffraction (SAED) pattern in Fig. 3d also confirms that the hybrid possesses an apparently polycrystalline characteristic. On the basis of the above structural information, it is obvious that high-quality phase junctions between wurtzite CdS and zinc-blende CdS are successfully achieved through current one-step hydrothermal method.

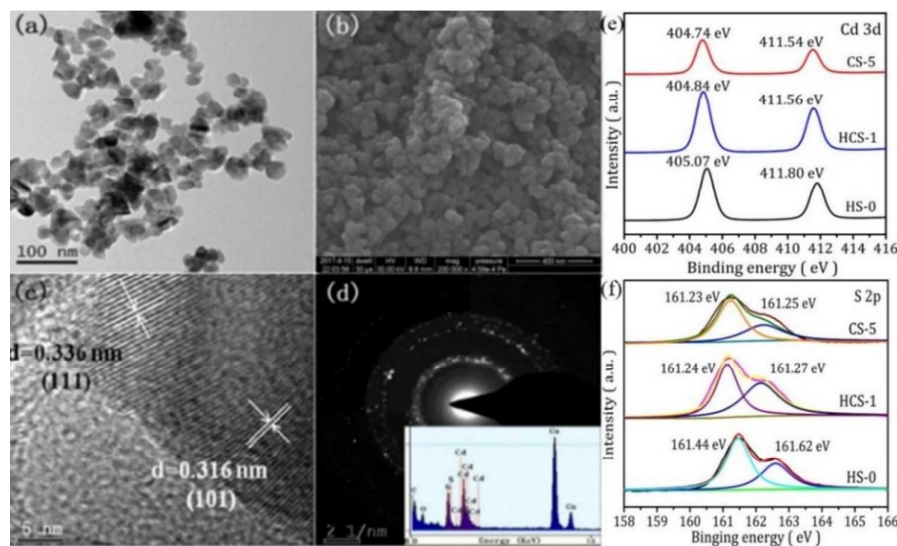


**Fig. 3** Typical large-area TEM (a) and SEM (b) images of the HCS-1 sample. HRTEM image (c) and corresponding SAED pattern (d) of the HCS-1 sample. Insert in panel (d) is the EDX spectrum of the heterostructured HCS-1 sample. High-resolution XPS spectra of Cd 3d (e) and S 2p (f) of HS-0, HCS-1, and CS-5.

The further detail of the samples on surface composition and chemical state were also investigated by XPS technique and the corresponding results are displayed in Fig. 3e and 3f. In Fig. 3e, the Cd 3d XPS spectrum of HS-0 gives two characteristic peaks located at 405.07 and 411.80 eV, which could be assigned to Cd 3d<sub>5/2</sub> and Cd 3d<sub>3/2</sub>, respectively.<sup>33</sup> In addition, it is observed from Fig. 3f that the two main peaks at 161.44 eV and 161.62 eV can be attributed to the S 2p<sub>3/2</sub> and S 2p<sub>1/2</sub>, respectively, indicating that the valence state of element S is  $-2$ .<sup>34</sup> However, the Cd 3d and S 2p peak positions in the HCS-1 hybrid and CS-5 moved slightly toward the lower binding energy compared to HS-0 (Fig. 3e and 3f) in turn. This is probably because the HS-0 contains pure wurtzite CdS phase and CS-5 almost own a zinc-blende CdS phase. On the contrary, the heterostructured HCS-1 sample has a mixture phase of zinc-blende CdS and wurtzite CdS. Thus, the different crystal structures of HCS-1 are responsible for the differences in their chemical environment, which is consistent with the XRD and TEM results reported above. In addition, this phenomenon was also observed in the XPS results of m-BiVO<sub>4</sub>/t-BiVO<sub>4</sub> heterostructures.<sup>23</sup>

Photocatalytic CO<sub>2</sub> conversion to solar fuel is an extremely attractive approach to store solar energy in the form of chemical fuel. Therefore, the heterostructured HCS-*n* samples were expected to use in the reaction of CO<sub>2</sub> reduction with H<sub>2</sub>O under visible-light irradiation. The controlled blank reactions were firstly performed without light irradiation or in the absence of the photocatalyst, and no products were detected. The effect of various H<sub>2</sub>O amount on photocatalytic activity was also investigated and shown in Fig. 4. Only small amount of CH<sub>4</sub> and CO over HCS-1 was obtained in the absence of H<sub>2</sub>O. Whereas, once water was added, aside from CH<sub>4</sub> and CO obtained by CO<sub>2</sub> reduction, H<sub>2</sub> was also detected. Especially, the H<sub>2</sub>-evolving rate increases with increase in H<sub>2</sub>O content, and gas-generation (CO and CH<sub>4</sub>) rate conversely decreases in the CO<sub>2</sub> reduction process. This is mainly because H<sub>2</sub>O can not only serve as an electron donor and hydrogen source for the photocatalytic CO<sub>2</sub> reduction, but also it can also act as a competing reagent in a CO<sub>2</sub> photoreduction system and compete favorably for the electrons and produce the preferential generation of H<sub>2</sub>.<sup>35,36</sup> It is obvious that water content based on the competitively reaction kinetics of

between CO<sub>2</sub> photoreduction and H<sub>2</sub>O splitting to hydrogen is vital for the formation of CH<sub>4</sub> and CO under present CO<sub>2</sub> photoreduction system.

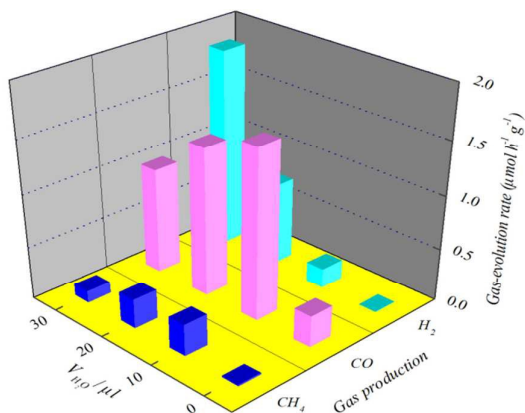


**Fig. 4** Gas-evolution (CH<sub>4</sub>, CO, and H<sub>2</sub>) rate from different amount of H<sub>2</sub>O over HCS-1 under visible-light irradiation ( $\lambda \geq 420$  nm).

To further gain insight into the effect of CdS heterostructure-based phase junction for CO<sub>2</sub> photoreduction reaction, photocatalytic performances of series of mixed-phase CdS samples was tested. Fig. 5a and 5b show the evolution of main products (CH<sub>4</sub> and CO) as a function of reaction time over various CdS-based photocatalysts prepared with various TEOA usages. From the curves, the yield of both CH<sub>4</sub> and CO over each catalyst increase

proportionally with the reaction time. However, it should be noted that all the heterostructured HCS-n samples exhibits markedly enhanced photocatalytic activity than pure HS-0, CS-5, and HS-0+CS-5 by physical mixing. Among these heterostructured CdS samples, the HCS-1 displays the highest CH<sub>4</sub>- and CO-evolving activity. According to the results of column of CO and CH<sub>4</sub> evolution rates versus various CdS samples induced by TEOA (Fig. 5c), and the maximal rate of CO evolution over HCS-1 up to 1.61  $\mu\text{mol h}^{-1} \text{g}^{-1}$ , correspondingly the maximal rate of CH<sub>4</sub> evolution is ca. 0.31  $\mu\text{mol h}^{-1} \text{g}^{-1}$ . The calculated yields of main products for the HCS-1 is nearly 27 times higher than that of the pure HS-0 sample. Meanwhile, the yields of both CO and CH<sub>4</sub> over HCS-1 is also almost 16 times greater than that of the CS-5 consisting of the mounting percentage of the zinc-blende CdS. The photocatalytic activity decreased in the order of HCS-1 > HCS-0.5 > HCS-2 > HCS-3 > HCS-0.1 > HS-0+CS-5 > CS-5 > HS-0 (Fig. 5c and Fig. S2). Obviously, the higher CH<sub>4</sub>- and CO-evolving rate of the HCS-1 sample may derive from coexistence of optimized phase junctions between zinc-blende CdS with wurtzite CdS. However, it is noteworthy that further increasing zinc-blende through more TEOA dosage leads to a slow reduction of photocatalytic CH<sub>4</sub>- and CO-producing activity. Therefore, this result allows us to realize the surface-phase junction affection that can play dominant roles in promoting photogenerated charges separation and migration.<sup>18-20</sup> Additionally, when the heterostructured CdS samples prepared by other alkali liquors (e.g. NH<sub>3</sub>·H<sub>2</sub>O, EDA, NaOH) instead of HCS-1 was used, these mix-phase CdS samples also show similar photocatalytic activities for converting CO<sub>2</sub> into CH<sub>4</sub> and CO (Fig. 5d) in the presence of water vapor.

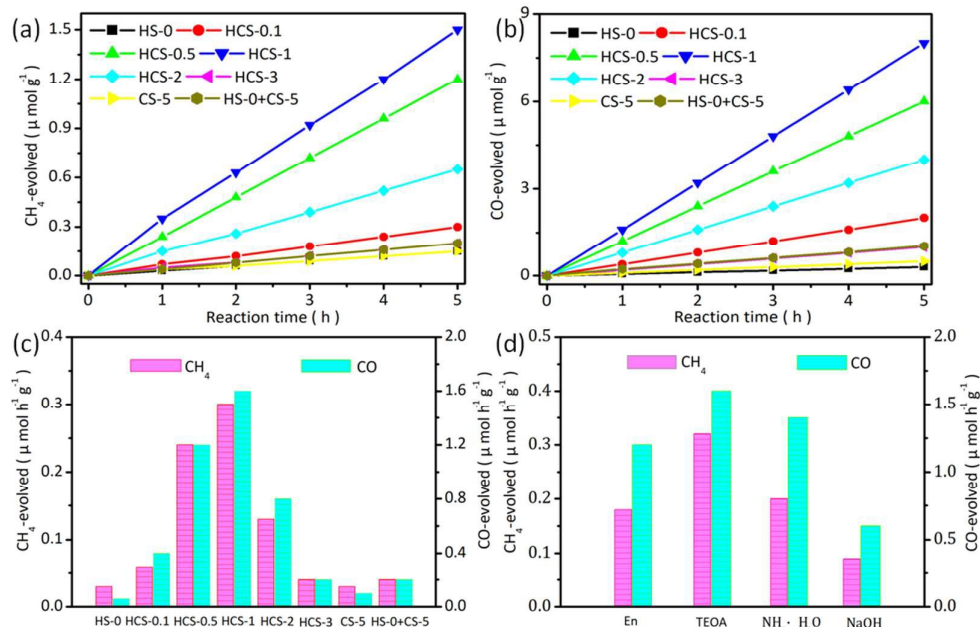


**Fig. 5** The photocatalytic performances of CdS samples prepared at different amounts of TEOA: (a) CH<sub>4</sub> production and (b) CO production, (c) CH<sub>4</sub>- and CO-evolution rate. (d) Gas-evolution (CH<sub>4</sub> and CO) rates of heterostructured CdS samples prepared in the presence of TEOA, EDA, NH<sub>3</sub>·H<sub>2</sub>O, and NaOH.

The photocatalytic stability of the as-prepared heterostructured HCS-1 hybrids was also investigated, and the corresponding result

of the repeated cycled testing is shown in Fig. 6a. Notably, the optimized HCS-1 sample presents excellent photocatalytic stability

during CO<sub>2</sub> photoreduction process, without hardly obvious changes in activity after 100 h stability test under the same reaction conditions. In this study, to verify the cause of long photocatalytic lifetime, the stability of mixed-phase CdS surface-phase junction with suitable bonding region was investigated by HRTEM and XRD. On the basis of the HRTEM (Fig. 6b) and XRD (Fig. 6c) after 100 h reaction times, it can be found that the stable chemical composition and phase junction of the HCS-1 nano hybrid was still maintained. The results demonstrated that the phase junction is very stable during photocatalytic reaction process, and chemical composition of CdS remains unchanged by prolonging irradiation time. The unprecedented photostability may be related to the suitable bonding region width, which can be the shield for phase junction.<sup>32</sup> In view of these experimental results, the heterostructured CdS-based nano hybrid exhibits undoubtedly the unique advantages of facile fabrication, tunable heterointerfaces, high CH<sub>4</sub>-/CO-producing activity and durably long lifetime, which make it a competitive candidate as a sulfide photocatalyst for converting CO<sub>2</sub> into solar-fuel owing to the high-quality and facily synthesized CdS phase junctions.

In order to explore the nature of differences in photocatalytic activities of different CdS photocatalysts, the physicochemical

characterization of the series of CdS samples were conducted. As displayed in Fig. S3, it is evidence that the particle size cannot responsible for the difference of photocatalytic activity of CdS-based nano hybrids because of their similar values. Subsequently, the optical properties of samples were examined by UV-visible diffuse reflectance spectra (DRS). The optical absorption properties of the as-prepared HCS-1 sample are shown in Fig. 7a, along with these of the HS-0 and CS-5 obtained for comparison. According to the DRS results, the HS-0 sample had a band gap of 2.20 eV, corresponding to an optical absorption edge of ca. 560 nm. However, the band gap value of CS-5 sample was deduced to be 2.30 eV, corresponding to an optical absorption edge of about 539 nm. Apparently, as comparison with HS-0 and CS-5 samples, heterostructured HCS-1 sample on the absorption edge is calculated to be ca. 550 nm that is lower than that of the value of absorption edge of HS-0 and larger than the absorption edge value of CS-5. This result confirms the coexistence of two crystalline phases of CdS. As for HCS-1, it should be pointed out that the optical absorption intensity of HCS-1 sample is higher than that of the isolated CdS sample. The difference in photo-absorption may be also originated from the unique junctions between zinc-blende CdS and wurtzite CdS in this composition.<sup>23</sup>

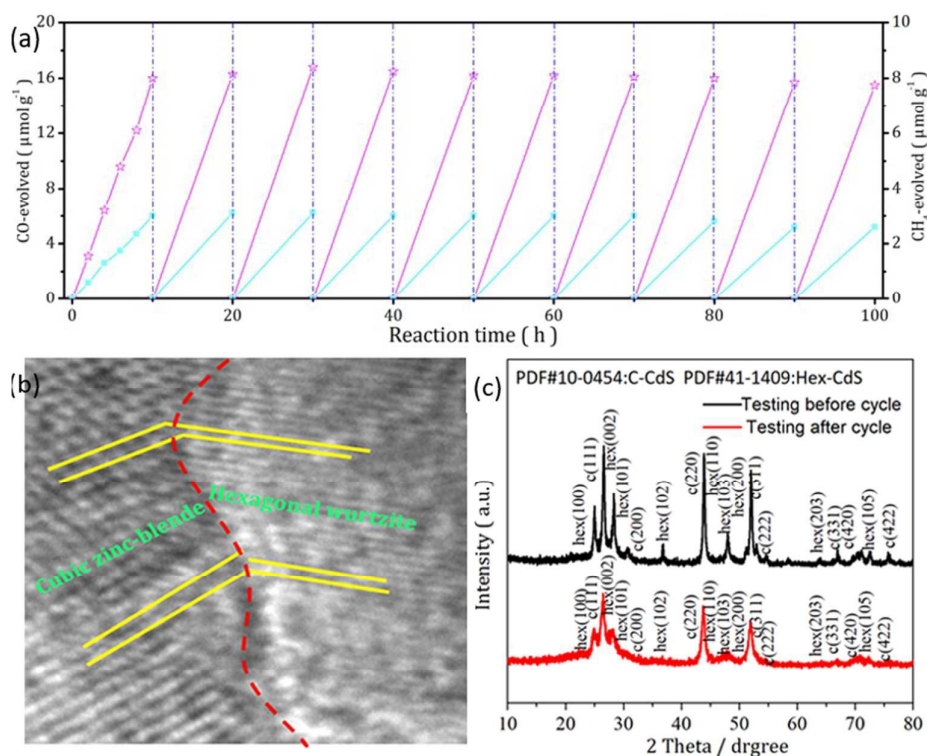


**Fig. 6** (a) The photocatalytic stability of HCS-1 under visible-light irradiation ( $\lambda \geq 420$  nm). (b) The HRTEM images of the HCS-1 after irradiation for 100 h. (c) XRD patterns of HCS-1 before and after the irradiation for 100 h.

Additionally, to understand the electronic band structure of heterostructured HCS-n sample, valence band XPS (VB XPS) was used for the observation of the valence band electronic state of these as-prepared samples (Fig. 7b). It is estimated that the valence band ( $E_{VB}$ ) potentials of HS-0, HCS-1, and CS-5 are ca. 1.51 V, 1.30 V, and 1.32 V in turn. Wherefore, the

conduction band potential ( $E_{CB}$ ) of HS-0, HCS-1, and CS-5 is estimated at about -0.69 V, -0.95, and -1.00, respectively, obtained by the  $E_g = E_{VB} - E_{CB}$ . The difference in the conduction-band potentials for the two phases can be also revealed by measuring the flat-band potentials of CdS samples. The Mott-Schottky plots for HS-0, HCS-1, and CS-5 film in 0.5 mol/L

$\text{Na}_2\text{SO}_4$  solution (pH=7) were given in Fig. 7c. On the basis of the Mott–Schottky analysis, the flat-band potentials ( $E_{fb}$ ) of HS-0, HCS-1, and CS-5 are  $-0.59$  V,  $-0.62$  V, and  $-0.72$  V vs. SCE ( $-0.35$  V,  $-0.38$  V, and  $-0.48$  V vs. NHE), respectively. As far as the n-type semiconductors are concerned, generally speaking, their conduction band potentials ( $E_{CB}$ ) in values are more negative than those of corresponding  $E_{fb}$  and is considered to be located on top of the  $E_{fb}$  (0.1–0.2 V more negative).<sup>37,38</sup> In view of this, it is estimated that conduction band potentials ( $E_{CB}$ ) of HS-0, HCS-1, and CS-5 are ca.  $-0.65$  V,  $-0.72$  V, and  $-0.82$  V, respectively, which was less than the redox potential of CO/CO<sub>2</sub> ( $-0.53$  V vs NHE, at pH 7.00).<sup>23</sup> These values are close to the conduction band potentials derived from the valence band. These results show that the conduction band potential of HS-0 is more positive than that of

CS-5, and the valence band potential of CS-5 is less negative than that of HS-0. Thus, a band structure based on the type II heterojunction<sup>7</sup> can be formed in CdS nanostructures consisting of wurtzite and zinc-blende CdS (Fig. 7d). Once CdS is activated by the photon energy to form electrons and holes, the type II heterojunction can drive the electrons and holes near surface to flow in opposite direction between HS-0 and CS-5 through the junction channel by the potential difference, while the high-quality phase junction from HCS-1 could serve as an active site to drive more photo-generated holes to drift into valence band of wurtzite CdS and promote the separation of charge carriers more effectively, which therefore enhance their photocatalytic CO and CH<sub>4</sub> evolution performances and decrease the photocorrosion rate of CdS photocatalysts for reaction kinetics..

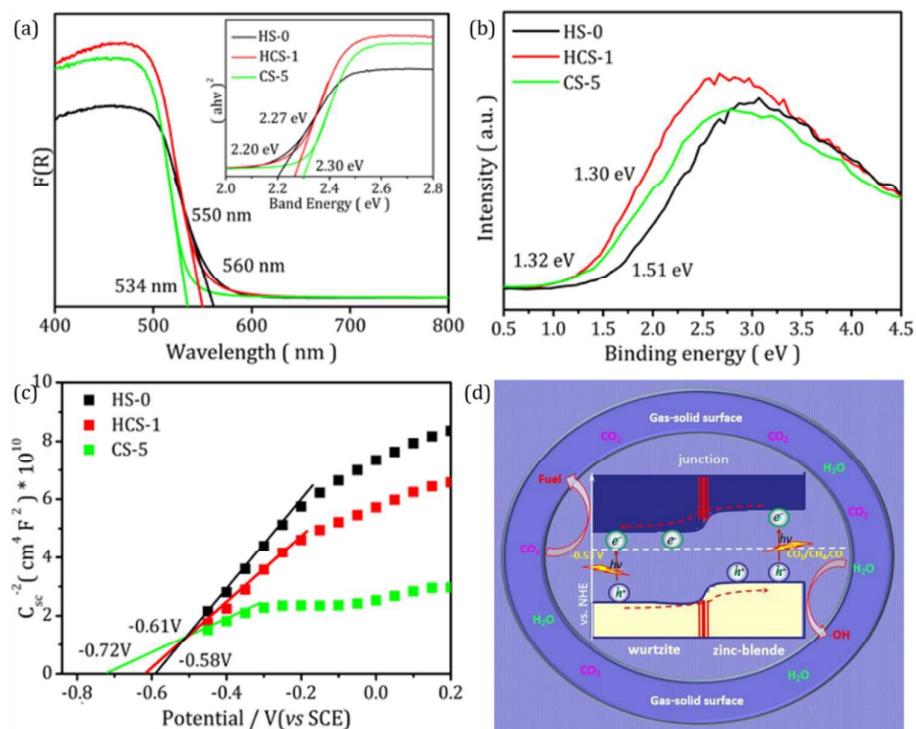


**Fig. 7** (a) Diffuse absorption spectra of the various CdS samples. The insert is the optical band gap energy  $E_g$  of the corresponding CdS samples. (b) Valence-band XPS spectra of various CdS samples. (c) Mott-Schottky plots obtained for the films electrodes prepared by various CdS samples in 0.2 M  $\text{Na}_2\text{SO}_4$ . (d) Scheme for electron–hole transfer between the zinc-blende and wurtzite CdS phases in the surface-phase junction.

The photo-electrochemical characterization was performed to further confirm that the mixed-phase CdS heterostructure has a better ability to transfer generated charge carrier (Fig. 8a). As compared to HS-0 and CS-5, heterostructured HCS-1 gives the superior transient photocurrents under visible light illumination. Of special note that the transient photocurrent intensities of these CdS-based samples are consistent with the photocatalytic CH<sub>4</sub>/CO-evolving rates reported above (Fig. 5). It is obvious that the optimum heterointerface mediated by zinc-blende CdS and wurtzite CdS in the hybrid can promote photo-generated electron/hole migrating, suggesting the efficient photo-induced charge separation and transfer occurring on the heterostructured HCS-1 sample.

Additionally, the Nyquist plots of the impedance data of samples were studied in order to further reveal the charge transfer process. As presented in Fig. 8b, the charge-transfer resistance of HCS-1 sample significantly decreased in the middle-frequency region as compared with those of HS-0 and CS-5 samples, according to the semicircles provided these CdS film electrodes, demonstrating a diminution in the electron recombination time. This EIS analysis indicates that the more efficient transfer of photo-generated carriers as a cooperative result of the junctions between zinc-blende and wurtzite CdS is demonstrated. Therefore, the CdS-based phase junctions can effectively reduce the rapid recombination rate of electron–hole pairs within photocatalytic materials and prolong

the electron lifetime efficiently. As a result, more effective charge separation and transfer as well as higher photocatalytic performance were achieved.

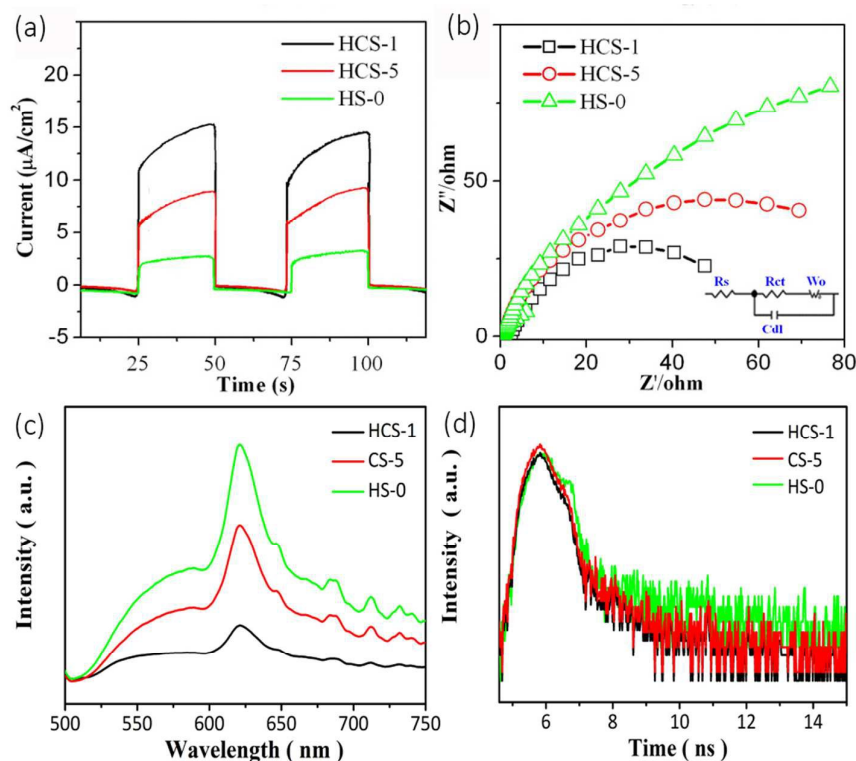


**Fig. 8** (a) The periodic on/off photocurrent response and (b) the Nyquist impedance plots of the as-prepared samples under visible-light irradiation. (c) The steady-state photoluminescence (PL) and (d) time-resolved transient-state photoluminescence (TRPL) spectra for HCS-1, CS-5, and HS-0 at ambient temperature, respectively.

The photoluminescence (PL) emission spectra were further employed to offer helpful information on the transfer and recombination of photo-generated charge carriers. Generally, the fluorescence emission results from the charge recombination, the less charge-recombination rate means the lower fluorescence. As shown in Fig. 8c, the broad fluorescence peaks for HCS-1, CS-5, and HS-0 located at  $\sim 550$  nm are related to the near band-edge emission of CdS,<sup>39</sup> and the band-gap emission peak on CS-5 sample exhibit a certain extent of blue shift in comparison with that of HCS-1, indicating that CS-5 sample has a greater band gap than HCS-1. This is also demonstrated through DRS results reported above (Fig. 7a). Additionally, the sharp fluorescence peaks for HCS-1, CS-5, and HS-0 centered at  $\sim 623$  nm are related to the trap-state recombination.<sup>37</sup> On the basis of preceding XRD results (Fig. 1), we observe that as the TEOA dosage was increased from 1 g to 5.0 g, the wurtzite CdS phase in heterostructured HCS-1 is decreases gradually, but zinc-blende phase increases gradually. Obviously, a strong emission demonstrated by the high PL peak on CS-5 can be realized to boost recombination of photoexcited charges because of superfluous lattice defects provided by S.<sup>40</sup> As compared to the CS-5 sample, the much lower PL peak of heterostructured HCS-1 indicates that photoexcited charges on HCS-1 can be effectively utilized and the charge carriers are favorable to migrate to the initiate CdS heterointerface formed by the wurtzite and zinc-blende

CdS. This result also indicates that the high-quality phase junctions endowed by wurtzite and zinc-blende CdS can effectively retard electron-hole recombination and promote the interfacial charge-carriers transport,<sup>8,32</sup> leading to more electrons to involve in reducing CO<sub>2</sub> into CO and CH<sub>4</sub>. In addition, further evidence comes from the time-resolved transient-state photoluminescence (TRPL) spectra tests (Fig. 8d). The TRPL tests reveal that the decay lifetime of charge carriers in HCS-1 is shorter than those of CS-5 and HS-0, implying that the lifetime of photo-generated holes in HCS-1 might be very short and can be effectively utilized in the reactions rather than the recombination with the transferred electrons, thus inducing the best performance in the reactions of CO<sub>2</sub> reduction with H<sub>2</sub>O.

#### 4. Conclusions

In summary, heterointerface-tuned CdS photocatalyst composed of wurtzite CdS and zinc-blende CdS have been designed and fabricated by tuning the reaction parameters. The formation of the unique phase junctions is mainly determined by at present hydrothermal surroundings induced by TEOA on the basis of the TEOA-dependent in situ crystalline phase wurtzite/zinc-blende transition. In comparison with the isolate wurtzite CdS, the heterostructured CdS nanohybrids

own intimate heterointerfaces and stronger light absorptions as well as tunable band gaps, which are beneficial to improving charge separation efficiency and sunlight harvest, thus enhancing the ability of photocatalyst to convert CO<sub>2</sub> to CO and CH<sub>4</sub>. The synthetic strategy reported here will be not only helpful in systematically explore fabrication of heterointerface-tuned CdS nanocomposites but also provides a feasible approach for developing highly light-active photocatalysts for CO<sub>2</sub> conversion into renewable solar-fuels.

### Conflicts of interest

In accordance with our policy on Conflicts of interest please ensure that a conflicts of interest statement is included in your manuscript here. Please note that this statement is required for all submitted manuscripts. If no conflicts exist, please state that "There are no conflicts to declare".

### Acknowledgements

This study was supported by the National Natural Science Foundation of China (Grant no. 21463019), the National First-rate Discipline Project of Ningxia (Chemical Engineering and Technology NXYLXK2017A04), the Major Innovation Projects for Building First-class Universities in China's Western Region, the Natural Science Foundation of Ningxia Province (NZ17036).

### Notes and references

- 1 K. Li, B. Peng and T. Peng, Recent advances in heterogeneous photocatalytic CO<sub>2</sub> conversion to solar fuels. *ACS. Catal.*, 2016, **6**, 7485–7527.
- 2 L. Schmidt-Mende, J. K. Stolarczyk and S. N. Habisreutinger, photocatalytic reduction of CO<sub>2</sub> on TiO<sub>2</sub> and other semiconductors. *Angew. Chem. Int. Ed.*, 2013, **52**, 2–39.
- 3 H. Fujiwara, H. Hosokawa, K. Murakoshi, Y. Wada, S. Yanagida, T. Okada and H. Kobayashi, Effect of surface structures on photocatalytic CO<sub>2</sub> reduction using quantized CdS nanocrystallites. *J. Phys. Chem. B.*, 1997, **101**, 8270–8278.
- 4 W. Wang, S. Wang, X. Ma and J. Gong, Recent advances in catalytic hydrogenation of carbon dioxide. *Chem. Soc. Rev.*, 2011, **40**, 3703–3727.
- 5 B.-J. Liu, T. Torimoto and H. Yoneyama, Photocatalytic reduction of CO<sub>2</sub> using surface-modified CdS photocatalysts in organic solvents. *J. Photochem. Photobiol. A*, 1998, **113**, 93–97.
- 6 H. Kisch and P. Lutz, Photoreduction of bicarbonate catalyzed by supported cadmium sulfide. *Photochem. Photobiol. Sci.*, 2002, **1**, 240–245.
- 7 Z.-R. Tang, B. Han, C. Han and Y.-J. Xu, One dimensional CdS based materials for artificial photoredox reactions. *J. Mater. Chem. A*, 2017, **5**, 2387–2410.
- 8 K. Li, M. Han, R. Chen, S.-L. Li, S.-L. Xie, C. Mao, X. Bu, X.-L. Cao, L.-Z. Dong, P. Feng and Y.-Q. Lan, Hexagonal@ cubic CdS core@shell nanorod photocatalyst for highly active production of H<sub>2</sub> with unprecedented stability. *Adv. Mater.*, 2016, **28**, 8906–8911.
- 9 X. Y. Pan and Y. J. Xu, Graphene-templated bottom-up fabrication of ultralarge binary CdS–TiO<sub>2</sub> nanosheets for photocatalytic selective reduction. *J. Phys. Chem. C*, 2015, **119**, 7184–7194.
- 10 H. Park, H. H. Ou, A. J. Colussi and M. R. Hoffmann, Artificial photosynthesis of C<sub>1</sub>–C<sub>3</sub> hydrocarbons from water and CO<sub>2</sub> on titanate nanotubes decorated with nanoparticle elemental copper and CdS quantum dots. *J. Phys. Chem. A*, 2015, **119**, 4658–4666.
- 11 Y. C. Wei, J. Q. Jiao, Z. Zhao, W. J. Zhong, J. M. Li, J. Liu, G. Y. Jiang and A. J. Duan, 3D ordered macroporous TiO<sub>2</sub>-supported Pt@CdS core-shell nanoparticles: design, synthesis and efficient photocatalytic conversion of CO<sub>2</sub> with water to methane. *J. Mater. Chem. A*, 2015, **3**, 11074–11085.
- 12 G. X. Song, F. Xin, J. S. Chen and X. H. Yin, Photocatalytic reduction of CO<sub>2</sub> in cyclohexanol on CdS–TiO<sub>2</sub> heterostructured photocatalyst. *Appl. Catal. A*, 2014, **473**, 90–95.
- 13 J. Yu, J. Jin, B. Cheng and M. Jaroniec, A noble metal-free reduced graphene oxide–CdS nanorod composite for the enhanced visible-light photocatalytic reduction of CO<sub>2</sub> to solar fuel. *J. Mater. Chem. A*, 2014, **2**, 3407–3412.
- 14 J. E. Benedetti, D. R. Bernardo, A. Morais, J. Bettini and A. F. Nogueira, Synthesis and characterization of a quaternary nanocomposite based on TiO<sub>2</sub>/CdS/rGO/Pt and its application in the photoreduction of CO<sub>2</sub> to methane under visible light. *RSC Adv.*, 2015, **5**, 33914–33922.
- 15 L. L. Tan, W. J. Ong, S. P. Chai and A. R. Mohamed, Noble metal modified reduced graphene oxide/TiO<sub>2</sub> ternary nanostructures for efficient visible-light-driven photoreduction of carbon dioxide into methane. *Appl. Catal., B*, 2015, **166–167**, 251–259.
- 16 Y. C. Wei, J. Q. Jiao, Z. Zhao, W. J. Zhong, J. M. Li, J. Liu, G. Y. Jiang and A. J. Duan, 3D ordered macroporous TiO<sub>2</sub>-supported Pt@CdS core-shell nanoparticles: design, synthesis and efficient photocatalytic conversion of CO<sub>2</sub> with water to methane. *J. Mater. Chem. A*, 2015, **3**, 11074–11085.
- 17 X. Li, J. Chen, H. Li, J. Li, Y. Xu, Y. Liu and J. Zhou, Photoreduction of CO<sub>2</sub> to methanol over Bi<sub>2</sub>S<sub>3</sub>/CdS photocatalyst under visible light irradiation. *J. Nat. Gas. Chem.*, 2011, **20**, 413–417.
- 18 S. B. Wang and X. C. Wang, Photocatalytic CO<sub>2</sub> reduction by CdS promoted with a zeolitic imidazolate framework. *Appl. Catal., B*, 2015, **162**, 494–500.
- 19 J. Jin, J. G. Yu, D. P. Guo, C. Cui and W. K. Ho, A hierarchical Z-scheme CdS–WO<sub>3</sub> photocatalyst with enhanced CO<sub>2</sub> reduction activity. *Small*, 2015, **11**, 5262–5271.
- 20 L. B. Kuai, Y. Zhou, W. G. Tu, P. Li, H. J. Li, Q. F. Xu, L. Q. Tang, X. Y. Wang, M. Xiao and Z. G. Zou, Rational construction of a CdS/reduced graphene oxide/TiO<sub>2</sub> core-shell nanostructure as an all-solid-state Z-scheme system for CO<sub>2</sub> photoreduction into solar fuels. *RSC Adv.*, 2015, **5**, 88409–88413.
- 21 X. Wang, Q. Xu, M. Li, S. Shen, X. Wang, Y. Wang, Z. Feng, J. Shi, H. Han and C. Li, Photocatalytic overall water splitting

- promoted by an  $\alpha$ - $\beta$  phase junction on  $\text{Ga}_2\text{O}_3$ . *Angew. Chem. Int. Ed.*, 2012, **51**, 13089–13092.
- 22 J. Cheng, J. Feng and W. Pan, Enhanced photocatalytic activity in electrospun bismuth vanadate nanofibers with phase junction. *ACS Appl. Mater. Interfaces*, 2015, **7**, 9638–9643.
- 23 O. F. Lopes, K. T. G. Carvalho, A. E. Nogueira, W. Avansi Jr. and C. Ribeiro, Controlled synthesis of  $\text{BiVO}_4$  photocatalysts: Evidence of the role of heterojunctions in their catalytic performance driven by visible-light. *Appl. Catal. B: Environ.*, 2016, **188**, 87–97.
- 24 J. G. Hou, C. Yang, Z. Wang, W. L. Zhou, S. Q. Jiao and H. M. Zhu, In situ synthesis of  $\alpha$ - $\beta$  phase heterojunction on  $\text{Bi}_2\text{O}_3$  nanowires with exceptional visible-light photocatalytic performance. *Appl. Catal. B: Environ.*, 2013, **142–143**, 504–511.
- 25 J. F. Zhang, S. Wageh, A. Al-Ghamdi and J. G. Yu, New understanding on the different photocatalytic activity of wurtzite and zinc-blende CdS. *Appl. Catal. B: Environ.*, 2016, **192**, 101–107.
- 26 H. N. Kim, T. W. Kim, I. Y. Kim and S. J. Hwang, Cocatalyst-free photocatalysts for efficient visible-light-induced  $\text{H}_2$  production: porous assemblies of CdS quantum dots and layered titanate nanosheets, *Adv. Funct. Mater.*, 2011, **21**, 3111–3118.
- 27 J. Z. Chen, X. J. Wu, L. S. Yin, B. Li, X. Hong, Z. X. Fan, B. Chen, C. Xue and H. Zhang, One-pot synthesis of CdS nanocrystals hybridized with single-layer transition-metal dichalcogenide nanosheets for efficient photocatalytic hydrogen evolution. *Angew. Chem. Int. Ed.*, 2015, **54**, 1210–1214.
- 28 Y. P. Xie, Z. B. Yu, G. Liu, X. L. Ma and H.-M. Cheng, CdS-mesoporous ZnS core-shell particles for efficient and stable photocatalytic hydrogen evolution under visible light. *Energy Environ. Sci.*, 2014, **7**, 1895–1901.
- 29 L. J. Zhang, S. Li, B. K. Liu, D. J. Wang and T. F. Xie, Highly efficient CdS/ $\text{WO}_3$  photocatalysts: Z-Scheme photocatalytic mechanism for their enhanced photocatalytic  $\text{H}_2$  evolution under Visible Light. *ACS Catal.*, 2014, **4**, 3724–3729.
- 30 N. Bao, L. Shen, T. Takata, K. Domen, A. Gupta, K. Yanagisawa and C. A. Grimes, Facile Cd-thiourea complex thermolysis synthesis of phase-controlled CdS nanocrystals for photocatalytic hydrogen production under visible light. *J. Phys. Chem. C*, 2007, **111**, 17527–17531.
- 31 L. A. Silva, S. Y. Ryu, J. Choi, W. Choi and M. R. Hoffmann, Photocatalytic hydrogen production with visible light over Pt-interlinked hybrid composites of cubic-phase and hexagonal-phase CdS. *J. Phys. Chem. C*, 2008, **112**, 12069–12073.
- 32 Z. Z. Ai, G. Z., Y. Y. Zhong, Y. L. Shao, B. B. Huang, Y. Z. Wu and X. P. Hao, Phase junction CdS: high efficient and stable photocatalyst for hydrogen generation. *Applied Catalysis B: Environ.*, 2018, **221**, 179–186.
- 33 L. H. Zhang, F. Q. Sun, Y. B. Zuo, C. F. Fan, S. P. Xu, S. M. Yang and F. L. Gu, Immobilisation of CdS nanoparticles on chitosan microspheres via a photochemical method with enhanced photocatalytic activity in the decolourisation of methyl orange. *Appl. Catal. B: Environ.*, 2014, **156–157**, 293–300.
- 34 I. Majeed, M. A. Nadeem, M. Al-Oufi, M. A. Nadeem, G. I. N. Waterhouse, A. Badshah, J. B. Metson and H. Idriss, On the role of metal particle size and surface coverage for photocatalytic hydrogen production: A case study of the Au/CdS system. *Appl. Catal. B: Environ.*, 2016, **182**, 266–276.
- 35 A. Corma and H. Garcia, Photocatalytic reduction of  $\text{CO}_2$  for fuel production: Possibilities and challenges. *J. Catal.*, 2013, **308**, 168–175.
- 36 S. Sato, T. Arai and T. Morikawa, Toward solar-driven photocatalytic  $\text{CO}_2$  reduction using water as an electron donor. *Inorg. Chem.*, 2015, **54**, 5105–5113.
- 37 S. R. Morrison, *Electrochemistry at semiconductor and oxidized metal electrodes*, Plenum Press, New York, 1980.
- 38 L. H. Yu, X. Y. Zhang, G. W. Li, Y. T. Cao, Y. Shao and D. Z. Li, Highly efficient  $\text{Bi}_2\text{O}_2\text{CO}_3/\text{BiOCl}$  photocatalyst based on heterojunction with enhanced dye-sensitization under visible light. *Appl. Catal. B: Environ.*, 2016, **187**, 301–309.
- 39 T. Simon, N. Bouchonville, M. J. Berr, A. Vaneski, D. Volbers, R. Wywich, M. Doblinger, A. S. Sussha, A. L. Rsgach, F. Jakel, J. K. Stolarczyk and J. Feldmann, Redox shuttle mechanism enhances photocatalytic  $\text{H}_2$  generation on Ni-decorated CdS nanorods. *Nat. Mater.*, 2014, **13**, 1013–1018.
- 40 X.-L. Yin, L.-L. Li, W.-J. Jiang, Y. Zhang, X. Zhang, L.-J. Wan and J.-S. Hu,  $\text{MoS}_2/\text{CdS}$  nanosheets-on-nanorod heterostructure for highly efficient photocatalytic  $\text{H}_2$  generation under visible light irradiation. *ACS Appl. Mater. Interfaces*, 2016, **8**, 15258–15266.

**TEOA-induced in situ formation of wurtzite and zinc-blende CdS heterstructures as  
a high-active and long-lasting photocatalyst for converting CO<sub>2</sub> into solar fuel**

Yao Chai, Jiaxue Lu, Li Li,\* Deli Li, Meng Li, and Jun Liang\*

*State Key Laboratory of High-efficiency Utilization of Coal and Green Chemical  
Engineering, College of Chemistry and Chemical Engineering, Ningxia University,  
Yinchuan 750021, China.*

